

Microstructural Refinement of Bainite and Martensite for Enhanced Strength and Toughness in High-Carbon Low-Alloy Steel

J. CHAKRABORTY, P.P. CHATTOPADHYAY, D. BHATTACHARJEE, and I. MANNA

This study attempts to determine the scope and extent of microstructural refinement through complete/partial recrystallization of prior cold deformed ferrite during austenitizing (1223 K (950 °C), 15 minutes) and/or austempering (543 K (270 °C), 30 minutes) followed by water quenching to obtain ultrafine bainitic sheaves along with thin martensitic plates in SAE 52100 steel. The volume fraction and sheaf/plate dimension (thickness/length) of bainitic ferrite and martensite were determined by optical and scanning/transmission electron microscopy studies coupled with compositional microanalysis. Marginal improvement in the tensile strength and significant improvement in the impact properties is obtained at an optimum level of prior cold deformation by tension in comparison to that recorded in austempered condition without prior deformation.

DOI: 10.1007/s11661-010-0288-1

© The Minerals, Metals & Materials Society and ASM International 2010

I. INTRODUCTION

CONVENTIONALLY quenched and tempered martensitic SAE 52100 steel is a very popular grade of high-carbon low-alloy steel for various structural applications, mostly as small, medium, and large ball and roller bearings for automobile applications and also for medium and heavy duty engineering components.^[1] The strength of the martensitic matrix coupled with the high amount of primary alloy carbides provides resistance to both abrasive and adhesive wear encountered in bearing assemblies. However, high strain and strain rate loads of cyclic nature warrant greater tensile strength and toughness.^[2] Recently, we have demonstrated that bainite-martensite duplex microstructure obtained through austempering followed by quenching route yields superior mechanical properties as compared to that developed by conventionally quenched and tempered martensitic structure in SAE 52100 steel without/prior cold deformation.^[3,4]

The present study aims to further increase the scope and extent of improving strength and toughness of this steel by aiming to refine the dimension (length or thickness) of bainitic sheaves and martensite plates through controlled cold deformation prior to austenitization and

partial austempering followed by quenching to room temperature. Young and Bhadeshia^[5] asserted that the presence of a soft phase embedded in a hard matrix is conducive to enhance toughness in steel. The conventional Hall–Petch relationship coupled with the effects of both substitutional and interstitial solid solution strengthening, work hardening, and second-phase spacing is summarized by the following equation:

$$\sigma = \sigma_{\text{Fe}} + \sigma_c + \sum \sigma_{\text{ss}} + K_1(L_3)^{-1} + K_2\rho_d^{1/2} + K_3\Delta^{-1} \quad [1]$$

where σ_{Fe} is the strength of pure annealed iron; σ_c is the contribution of solid solution strengthening due to carbon; $\sum \sigma_{\text{ss}}$ is the sum of contributions to solid solution strengthening from all substitutional solutes; L_3 is the ferrite plate thickness; ρ_d is the dislocation density; Δ is the average distance between primary carbide particles; and K_1 , K_2 , and K_3 are material constants.

In order to reduce L_3 , an attempt has been made to decrease the prior austenite grain size by austenitization preceded by varying degrees of cold deformation. Several studies in the past have investigated the effect of austenite grain size on the bainitic transformation kinetics and morphology.^[6–9] Barford and Owen^[6] and Umemoto *et al.*^[7] reported that the bainitic transformation rate increases when grain size is decreased, as greater specific grain boundary area provides heterogeneous nucleation sites and promotes austenite to bainite transformation. On the other hand, Graham and Axon^[8] suggested that the growth of bainite is retarded when austenite grains are finer due to physical restriction to sheave growth by grain boundaries. Matsuzaki and Bhadeshia^[9] observed that the refinement in the austenite grain size leads to acceleration in the rate of transformation, but the overall reaction kinetics are limited by a slow growth rate or extent.

J. CHAKRABORTY, Research Scholar, is with the Department of Metallurgical and Materials Engineering, Indian Institute of Technology, Kharagpur, W.B. 721 302, India, and Manager-Metallography, Scientific Services and Research and Development, Tata Steel, Jamshedpur 831 001, Jharkhand, India. P.P. CHATTOPADHYAY, Professor, is with the Department of Metallurgy and Materials Engineering, Bengal Engineering and Science University (BESU), Sibpore, Howrah 711103, India. D. BHATTACHARJEE, Director, is with Scientific Services and Research and Development, Tata Steel. I. MANNA, Professor, is with the Department of Metallurgical and Materials Engineering, Indian Institute of Technology. Contact e-mail: imanna@metal.iitkgp.ernet.in

Manuscript submitted October 11, 2009.

Article published online July 21, 2010

Thus, lowering of prior austenite grain size may provide larger density of nucleation sites of bainite increasing the initial transformation rate, but the extent of sheave growth (or length and thickness) may eventually be stifled by the grain boundaries. In this connection, our recent study has indicated that this structural refinement of bainite due to smaller prior austenite grain size may indirectly restrict the formation of martensitic plates from residual austenite after controlled austempering followed by water quenching.^[4] However, a detailed evaluation of physical and mechanical properties with duplex microstructure was not feasible in that preliminary report. In view of this complex influence of grain size on bainite and martensite nucleation and growth, the present study further investigates the scope and extent of refinement of bainite and martensite duplex microstructure and its influence on the mechanical properties of interest in SAE 52100 steel.

II. EXPERIMENTAL

Three cylindrical samples of 10-mm diameter and 180-mm length of spheroidized annealed SAE 52100 steel having a nominal composition of 1.1 pct C, 1.46 Cr, 0.27 pct Si, 0.33 pct Mn, 0.14 pct V, 0.04 pct Ni, 0.02 pct P, and rest Fe (wt pct) were subjected to tensile elongations of 5, 10, and 15 pct, respectively, at room temperature in a universal tensile testing machine. The gripped ends of the samples were discarded. The remaining specimen samples of 10-mm thickness were cut and subjected to austenitizing at 1223 K (950 °C) for 15 minutes in an electrically heated furnace and then directly transferred to a salt bath furnace for austempering at 543 K (270 °C) for different time periods ranging from 10 to 70 minutes followed by instantaneous quenching to room temperature. The heat-treated samples were mechanically polished with up to 0.1- μ diamond paste and etched with nital (2 vol pct nitric acid in ethanol) for the purpose of optical and scanning electron microscopy studies. For transmission electron microscopy studies, the heat-treated samples were sectioned by a slow speed diamond cutter and mechanically polished up to 90- μ thickness. Three-millimeter discs were punched out from such thin samples and were subjected to twin-jet electropolishing using an electrolyte containing 15 pct perchloric acid and 85 pct ethanol at ambient temperature and 60 V (direct current) potential. Mechanical property in terms of hardness and tensile and impact strength of the samples having appropriate dimensions and geometry was measured using a Rockwell and Vickers hardness tester, universal testing machine, and Charpy impact tester, respectively. Analysis of the phase aggregate (identity, volume fraction, and crystallite size) and measurement of residual stress were carried out through X-ray diffraction (XRD) with a Panalytical X'pert PRO XRD (PANalytical, Almelo, The Netherlands) unit using Cu K_{α} radiation (0.154 nm). Nanoindentation tests were carried out using a CSM NHTX-55049 nanoindentation tester (CSM, Peseux Montbeliard, Doubs, Franche-Comte, France) coupled with an atomic force microscope

to estimate the elastic modulus and nanohardness of the constituent phases.

III. RESULTS AND DISCUSSION

Figure 1(a) shows a typical bainite + martensite duplex microstructure, obtained in SAE 52100 steel after austenitizing at 1223 K (950 °C) for 15 minutes followed by austempering at 543 K (270 °C) for

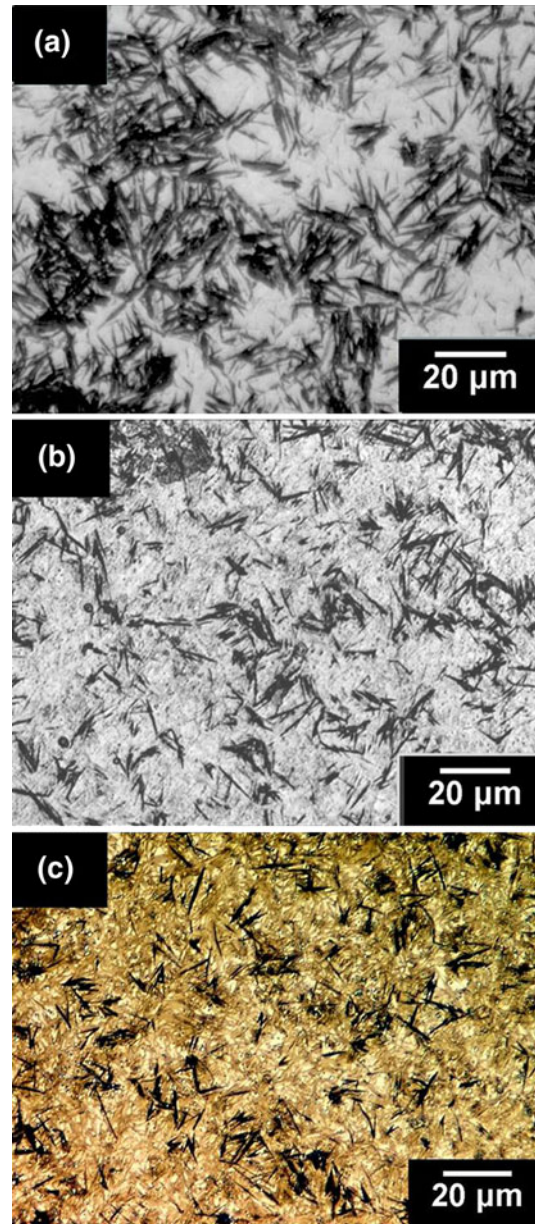


Fig. 1—(a) Optical micrograph showing bainitic sheaves along with martensitic laths/needles formed after partial austempering and quenching. (b) Optical micrograph showing smaller and thinner bainitic sheaves along with martensite obtained by partial austempering and quenching of prior cold deformed samples. (c) Color tinted view of (b), to reveal the identity of the phases/phase aggregates by their characteristic colors: martensite as yellow/straw, bainite as blue, and retained austenite as bright white.

30 minutes. Spearlike bainitic sheaves and narrow needlelike martensite plates, both dark etching, are uniformly distributed in the microstructure along with light etching retained austenite. Bainitic sheaves are relatively long and coarse. This microstructure is identical to that earlier reported by us.^[3] Figure 1(b) shows a similar optical microstructure of the same steel subjected to a similar austenitizing and austempering routine with 10 pct prior cold deformation by tension. It is apparent that the average bainitic sheaf length is smaller and thinner in Figure 1(b) than that in Figure 1(a). Careful image analysis reveals that the average sheaf length and thickness are 18 and 5 μm in Figure 1(a), whereas the same in Figure 1(b) are 10 to 12 μm and 2 to 3 μm , respectively. Furthermore, the light etching austenitic region is marginally smaller in Figure 1(b) than that in Figure 1(a). Thus, it is evident that prior cold deformation leads to the refinement of the bainite size and morphology and reduction in the amount of retained austenite.

Figure 1(c) is a color-tinted optical micrograph obtained after identical heat treatment as that for the sample whose microstructure is shown in Figure 1(b). The color contrast developed by modified Lopera etching^[10] reveals and identifies the microconstituents

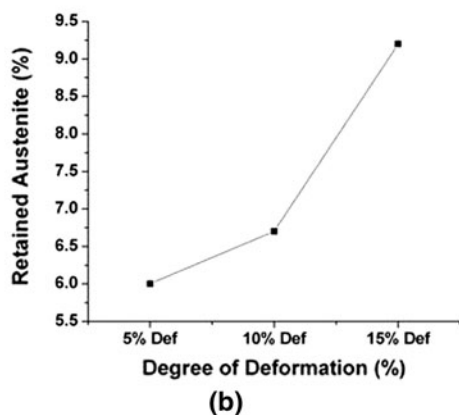
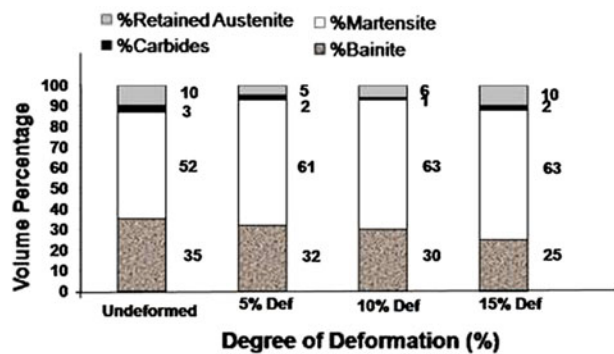


Fig. 2—(a) Relative volume fractions of various phases, determined by color metallography technique, obtained after different degrees of prior cold deformation. (b) The volume fractions of retained austenite (determined from XRD pattern using direct displacement method) as a function of prior cold deformation after austenitizing (1223 K (950 °C), 30 min) followed by austempering at 543 K (270 °C) for 30 min.

as bainite (blue spears/needles), martensite (straw colored needles), and retained austenite (bright regions), respectively. Figure 2(a) shows the volume percent of these phases determined from similar color micrographs of samples subjected to austempering for various time periods (15 to 120 minutes) at 543 K (270 °C) without or with prior cold deformation (by 5, 10, and 15 pct). It is apparent that the bainitic volume percent increases and both austenite and martensite volume percent decrease with increasing austempering time for samples without prior cold deformation. However, a reverse trend is observed in samples with increasing degree of prior cold deformation subjected to isochronal (30 minutes) austempering at the same temperature. It is expected that dislocation density increases with higher degree of cold deformation and leads to reduction in size of prior-austenite grains by recrystallization during austenitizing at 1223 K (950 °C) for 15 minutes. Since hardenability decreases with reduction in prior austenite grain size, it is anticipated that retained austenite amount should increase with greater amount of prior cold deformation, as seen in Figure 2(b). This reduction in bainite volume percent with increase in the degree of prior cold work may occur due to the hindrance to growth of ferritic sheaves by dislocation tangles (remaining after incomplete recrystallization) or grain boundaries (formed by recrystallization during austenitizing).^[11]

Figure 3 shows the typical morphology and dimensions of the ferritic sheaves within a predominantly bainitic area. This area contains a few spherical undissolved carbide particles. The average sheaf dimensions (length and width) match with that measured in Figure 1(b). Subsequent EDS analysis with ultrafine beam size allowed determination of the microcomposition of these spherical precipitates, giving an average composition of 8.75 pct C, 5.94 pct Cr, 0.80 pct Mn, and the rest Fe, which suggests that these phases are (FeCrMn)-C type mixed carbides partially dissolved or retained during austenitizing. This microstructural

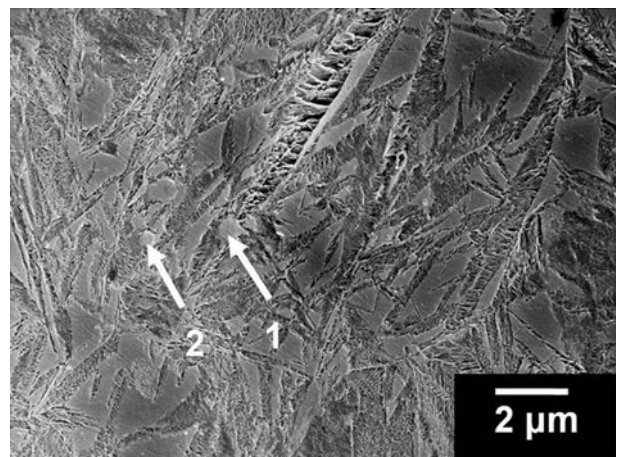


Fig. 3—SEM image of the prior cold deformed and austempered sample revealing primary carbides. EDS analysis at spots 1 and 2 allows compositional microanalysis of the phases (carbides) summarized in Table I.

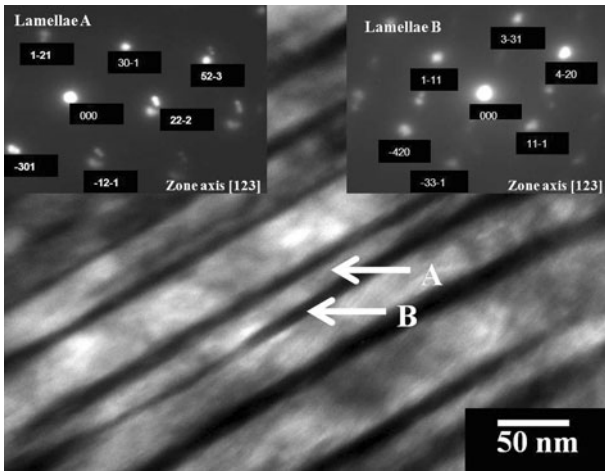


Fig. 4—Bright-field TEM image showing parallel stacks of ultrafine/nanometric ferrite plates (bright) of thickness <50 nm interspaced with thinner and darker austenite lamellae. Insets show the SAD pattern of typical ferritic (lamella A) and austenitic (lamella B) lamellae, respectively.

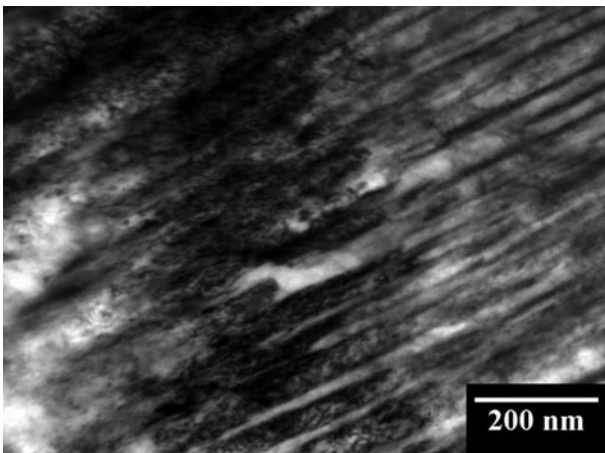


Fig. 5—Dense dislocation tangles revealed within bainitic ferrite sheaves indicating the presence of large stress field in the matrix retained after austenitizing or austempering.

feature is usual in bearing steel such as SAE 52100 and is beneficial to increase the abrasive or adhesive wear resistance for ball/roller bearing applications.^[1]

The bright-field TEM microstructure of samples subjected to 10 pct cold deformation (tensile) prior to austenitizing at 1223 K (950 °C) for 15 minutes, followed by austempering at 543 K (270 °C) for 30 minutes, shows typical bainitic regions (Figure 4). Here, the ferritic sheaves (bright) are less than 50-nm thick and uniformly interspaced with still thinner retained austenite lamellae (dark). The corresponding SAD analysis (shown as insets) confirms the bright (wider) and dark (thinner) regions as ferrite and austenite, respectively. Figure 5 reveals that some regions are populated with dense dislocation tangles. Due to the extremely small or nanometric thickness of the ferritic sheaves, it is anticipated that the dislocation activity/glide will be

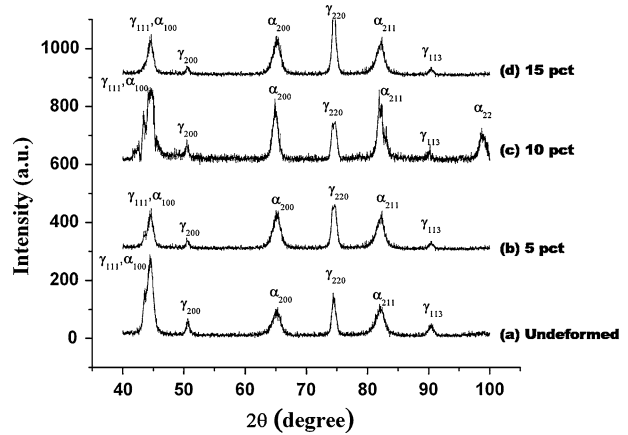


Fig. 6—Slow scan XRD profile of the SAE 52100 steel after austenitizing at 1223 K (950 °C) followed by isochronal austempering at 543 K (270 °C) for 30 min (a) without prior cold deformation and with (b) 5 pct, (c) 10 pct, and (d) 15 pct prior cold deformation. Note that the amount of retained austenite and ferrite and relative widths of the concerned peaks vary in different routines.

considerably restricted along the thickness direction that will eventually improve the strength level. The dislocation tangles are possibly retained due to incomplete recrystallization or may arise during austempering owing to transformational stresses. Figure 6 shows the XRD profiles of the samples austempered at 543 K (270 °C) without/with prior cold deformation (10 pct), for different austempering durations (15 or 30 minutes). This XRD profile, coupled with evidence from optical microscopy, suggests that the phase aggregate mainly comprises ferrite, martensite, cementite, and retained austenite. The relative integrated intensity and full-width at half-maximum of the major peaks of these phases are different for different conditions of austempering. Quantitative phase analysis on the basis of integrated intensity values of (200) peak of ferrite, per the direct comparison method,^[12] yields the relative amount of retained austenite, as shown in Figure 2(b).

As expected, the volume percent of bainite increased, while the amount of retained austenite and martensite decreased with increase in the austempering time. This is due to a greater degree of austenite to bainite transformation under isothermal conditions leading to reduction in the amount of retained austenite or martensite obtained after quenching to room temperature at the end of the austempering cycle. Furthermore, an increase in the amount of carbide with austempering time can be attributed to the same reason of greater degree of bainitic transformation and consequent increase in the amount of carbide on top of the volume percent of primary carbides present in the microstructure before austempering. Careful measurement of full-width at half-maximum of the ferrite peak, after necessary correction to eliminate peak broadening due to strain and instrumental error, indicates that the crystallite size of ferrite lies in the range 55 to 60 nm. The ferrite crystallite size is the maximum in the sample austempered at 543 K (270 °C) for 30 minutes after 15 pct prior cold deformation (~55 nm). It may be noted that

direct observation under TEM has earlier confirmed that the ferrite sheaf thickness is indeed 50 to 60 nm under similar conditions of austempering. Thus, the present exercise of austempering of cold deformed steel seems effective in restricting the ferritic sheaf size/thickness to less than 50 to 60 nm. These results lend direct credence to the proposition that bulk quantity of steel with nanometric sized microconstituents is possible in austempered steel.^[13] It is also worth noting that several ferrite peaks in Figure 5 show distinct evidence of splitting due to pronounced tetragonality of martensite formed due to quenching after austempering. Careful calculation of lattice parameters of martensite from the (200) and (002) indicates that the carbon content in martensite is relatively higher than that expected in martensite obtained in the same steel by the usual hardening treatment. The lattice parameters of martensite in the samples subjected to various degrees of prior cold deformation followed by austenitizing and austempering (30 minutes) are given in Table I.

Perhaps, extension of solid solubility due to smaller crystallite size of prior austenite (Gibbs–Thomson effect^[14]) and presence of significant dislocation density have contributed to retention of carbon in austenite prior to quenching at the end of austempering. This hypothesis is substantiated by the marginal increase in the amount of retained austenite when the degree of prior deformation is increased from 5 to 15 pct

(Figure 2(b)). It is relevant to mention that the amount of bainite marginally decreases with the increase in the prior cold deformation, mainly due to significant reduction in the amount of prior austenite grain size by recrystallization prior to austempering and consequent constriction of growth of ferrite due to small prior austenite grain size.

The lattice parameter of retained austenite is directly related to the dissolved carbon content in it. Careful determination of austenite peak and determination of austenite lattice parameters using Nelson and Riley analysis^[12] allowed estimation of carbon content in retained austenite at different stages of austempering. Figure 7(a) shows the variation of carbon content in retained austenite as a function of austempering time during austempering at 543 K (270 °C), following austenitizing of 15 pct prior cold deformed samples at 1223 K (950 °C) for 15 minutes.

This reduction in the carbon content is due to the precipitation of carbides from austenite that occurs concurrently with the formation of bainite through the usual eutectoid transformation mode. The progress of the latter transformation is reflected by reduction in volume percent of austenite with austempering time at 543 K (270 °C) (Figure 7(a)). Similar concurrent carbide precipitation from retained austenite in this alloy was earlier reported by us during austempering of samples without prior deformation.^[3] It has earlier been pointed out in Figure 2(a) that the volume fraction of bainite decreases while that of martensite increases with a higher degree of prior cold work, due to the smaller size of austenite grains formed during austenitizing at 1223 K (950 °C). Figures 2(a) and (b) further show that the volume fraction of retained austenite measured by image analysis and XRD marginally increases with the increase in degree of prior cold work. Possibly reduction in crystallite size leads to an increase in solubility of carbon in austenite due to the Gibbs–Thomson^[14] effect and aids in retention of austenite at room temperature. It is

Table I. Lattice Parameters (*a* and *c*) of Martensite as Obtained from the (200) and (002) Peaks in XRD Profile of Samples with Various Degrees of Prior Cold Deformation

Prior History	<i>c</i> (nm)	<i>a</i> (nm)
Undeformed	0.285	0.282
5 pct deformation	0.287	0.280
10 pct deformation	0.286	0.282
15 pct deformation	0.286	0.285

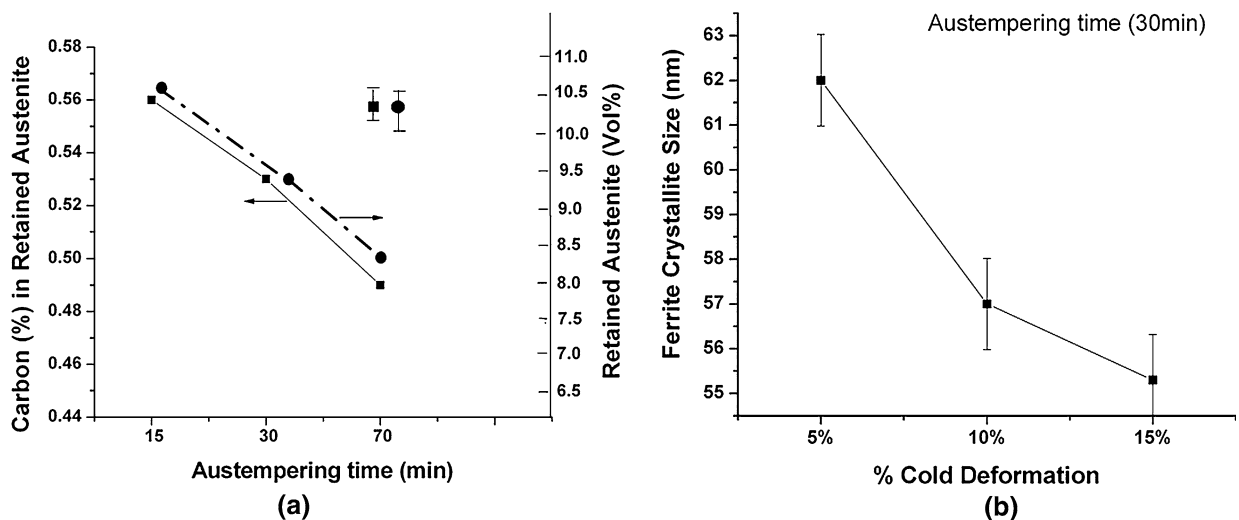


Fig. 7—(a) Variation of the retained austenite volume fraction (broken line) and carbon in it (solid line), with austempering time, in a 15 pct cold deformed sample. (b) Variation of ferrite crystallite size with degree of prior cold deformation for samples austempered at 543 K (270 °C) for 30 min. A steady decrease is observed with the increase in prior cold deformation.

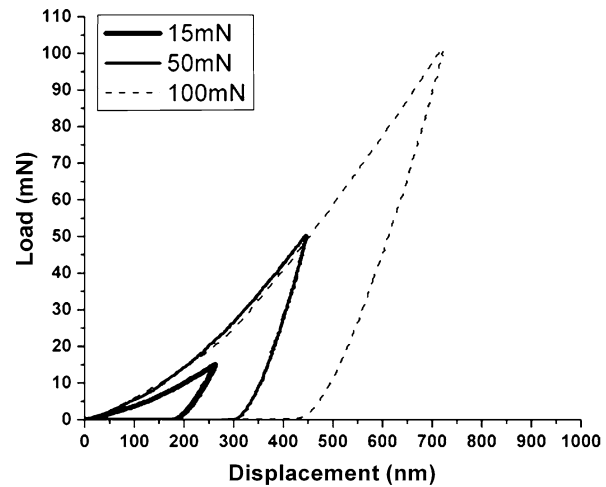
Fig. 8—(a) Load-displacement curves recorded with different levels of indentation load (15, 50, and 100 mN on bainitic sheaf in the same specimen). The shallower slope of the curve for 15 mN possibly indicates that the indentation was confined within the microconstituents or ferritic sheaf. (b) Load-displacement curves of three constituent phases under a constant load of 100 mN. Note that the stiffness is systematically lower for indentation made on martensite, bainite, and austenite, respectively. (c) Load-displacement curves of bainite in the undeformed and prior cold deformed (5, 10, and 15 pct) samples subjected to the same austenitizing (1223 K (950 °C)/15 min) and austempering (543 K (270 °C)/30 min) routine under an indentation load of 50 mN.

interesting to note that the crystallite size of ferrite (within bainite) decreases with the increase in degree of prior cold work (Figure 7(b)). Though the extent of decrease is marginal, the trend corroborates the earlier results of a decrease in bainitic volume percent with the increase in degree of prior cold work (confinement of ferritic sheaf within smaller prior austenite grain).

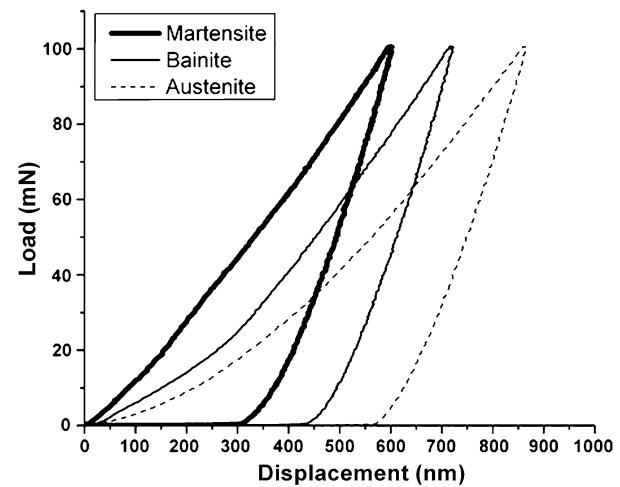
Figure 8(a) shows the response of the austempered steel to nanoindentation with different loads. The three indentations at three different loads were obtained on identical ferritic sheaves in the same microstructure obtained by austempering of 5 pct cold deformed samples at 543 K (270 °C) for 30 minutes. Since the applied load l (up to 100 mN) was below the yield strength, the elastic modulus could be calculated from the slope of the load displacement curve using the Oliver and Pharr equation.^[15] The elastic modulus was calculated to be 157 GPa (for $l = 15$ mN), 213 GPa (for $l = 50$ mN), and 210 GPa (for $l = 100$ mN). While the response to 50- and 100-mN loads is identical, the marginal difference of the same curve obtained with smaller load (15 mN) may be attributed to microstructural or compositional heterogeneity within the ferritic sheaves sensed by the ultra small extent of elastic strain caused by minimal magnitude of load.

Figure 8(b) presents another interesting feature of mechanical property related to the heterogeneity associated with the multiphase microstructure developed by the present routine of austempering. Nanoindentation on martensite, bainite, and austenite phases (located by careful microstructural study using the microscope coupled with the nanoindenter) yield three different load-displacement curves with distinctly different slopes during the loading cycle. Accordingly, the elastic modulus of the concerned phases were calculated using the same Oliver and Pharr relationship as 287 GPa (M), 210 GPa (B), and 162 GPa (RA) (marked in Figure 8(b)). It is worth noting that each strength (elastic modulus) data obtained from nanoindentation tests is associated with an average error margin of ± 5 GPa.

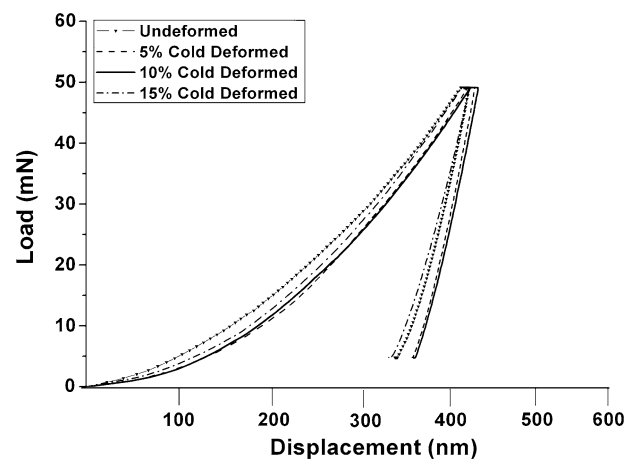
Figure 8(c) presents the effect of prior cold deformation on the elastic modulus of bainitic sheaves of the undeformed and prior cold deformed samples subjected to the same austenitizing (1223 K (950 °C)/15 minutes) and austempering (543 K (270 °C)/30 minutes) routine. A distinct difference in the slope is observed in the case of the undeformed sample as compared to the samples subjected to various degrees of prior cold deformation. The elastic modulus of the bainitic sheaves, as calculated by the Oliver and Pharr relationship, was calculated to be 246 GPa (undeformed), 210 GPa (5 pct prior cold



(a)



(b)



(c)

deformed), 223 GPa (10 pct prior cold deformed), and 229 GPa (15 pct prior cold deformed). The corresponding nanohardness of the same bainitic sheaves was 11.6 GPa (in undeformed condition), 8.5 GPa (5 pct prior cold deformed), 8.6 GPa (10 pct prior cold

deformed), and 8.7 GPa (15 pct prior cold deformed). Furnemont *et al.*^[18] and Jaques *et al.*^[19] reported nanohardness values of ~7 GPa of bainitic ferrite in a steel with about 0.29 to 0.30 wt pct carbon. In the present steel, the similar nanohardness value is substantially higher mainly because of the significantly higher initial carbon content (0.98 to 1.1 wt pct). It is interesting to note that despite having very high nanohardness, the elastic modulus of the bainitic sheaves, calculated from the nanoindentation tests, is lower in the case of the prior cold deformed samples as compared to the undeformed samples. It may be noted that prior deformation leads to significant reduction of sheaf thickness ferrite (in bainite) (Figure 4). Furthermore, the retained austenite volume fraction marginally increases with the degree of prior cold deformation. Thus, the presence of a greater amount of retained austenite interspaced between finer ferritic plates can lower the elastic modulus despite the ferritic plates being harder or stronger due to finer or thinner dimension.

Table II shows the variation of ultimate tensile strength of samples subjected to the identical routine of austenitizing and austempering. Table II allows the comparison of mechanical strength achieved under isochronal duration of austempering for an identical degree of prior cold work. It is apparent that the maximum strength is obtained after austempering for 30 minutes with 10 pct prior cold deformation. In general, prior cold deformation improves strength in all the cases up to 5 to 10 pct prior cold deformation but shows a lower strength at 15 pct prior cold deformation. The decrease in tensile strength of the 15 pct prior cold deformed sample may be attributed to the higher degree of dissolution of carbides during austenitizing leading to retention of a higher amount of austenite in the austempered and hardened condition. As a result, the volume fraction of both bainite and martensite

decreases, and consequently, the hardness and strength marginally drop in samples with a lower (5 to 10 pct) degree of prior cold deformation. The microhardness data of the specimens with a different degree of prior cold deformation (Table II) confirm the preceding inference. Thus, a higher amount of soft phase (retained austenite) interspaced between bainitic ferrite or martensite in the 15 pct prior cold deformed sample is responsible for the marginal decrease in hardness and strength.

Table II also records the variation of impact strength as a function of prior cold deformation for samples austempered at 543 K (270 °C) for 30 minutes. As noted earlier, for ultimate tensile strength, here again the impact strength remains the maximum at 10 pct prior cold deformation.

Figure 9 reveals residual dislocation tangles remaining in the ferritic areas after austempering. These

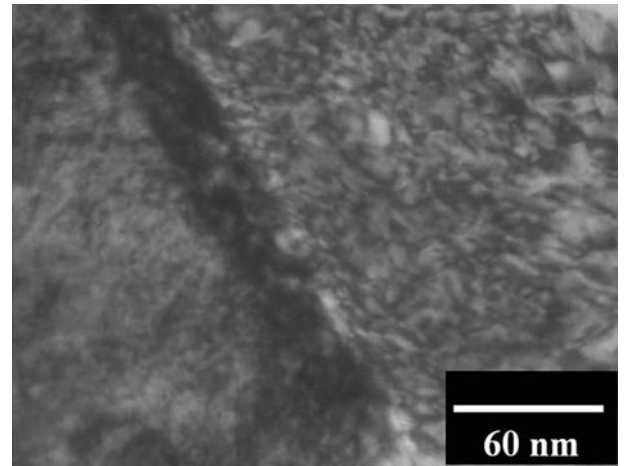


Fig. 9—TEM image showing dislocation tangles in a sample with 10 pct cold deformation prior to austenitizing at 1223 K (950 °C) followed by isochronal austempering at 543 K (270 °C) for 30 min.

Table II. Summary of Mechanical Properties as a Function of Austempering Time (at 543 K (270 °C)) and Degree of Prior Cold Deformation

Austempered Condition: Austempering Time (Min) (Austempered at 543 K (270 °C))	Degree of Deformation (Pct)	UTS (MPa)		Microhardness (Converted to HRc)		Impact Strength (Joules)
10 min	0	2200 ± 5 MPa		—	—	—
	5	2217 ± 5 MPa		—	—	—
	10	2230 ± 5 MPa		—	—	—
	15	2211 ± 5 MPa		—	—	—
30 min	0	2235 ± 5 MPa		B = 59.5	M = 63.0	53.0
	5	2247 ± 5 MPa		B = 57.0	M = 62.5	71.0
	10	2249 ± 5 MPa		B = 57.0	M = 62.0	73.0
	15	2200 ± 5 MPa		B = 58.0	M = 60.0	73.5
70 min	0	2210 ± 5 MPa		—	—	—
	5	2221 ± 5 MPa		—	—	—
	10	2213 ± 5 MPa		—	—	—
	15	2205 ± 5 MPa		—	—	—
Conventional hardened and tempered (austenitizing at 1123 K (850 °C) for 15 min; quenching to 493 K (220 °C) for 15 min, and tempering at 443 K (170 °C) for 60 min)	0	2210 to 2215 ^[17]		61 HRc ^[17]		43 to 47 ^[16]

B = bainitic sheaf.
M = martensite plate/lath.

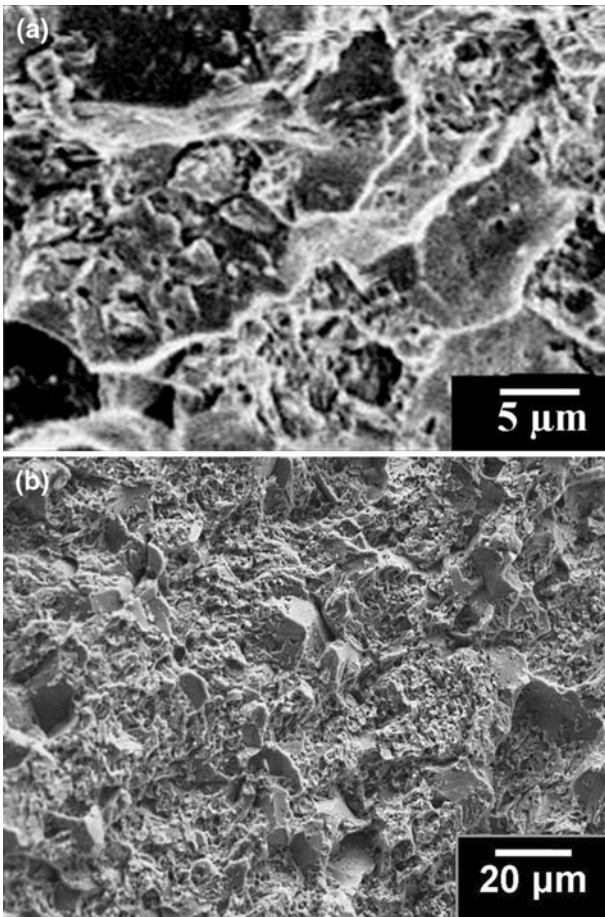


Fig. 10—(a) Fractograph of the sample as obtained after tensile testing of a 15 pct prior cold deformed sample subjected to austenitizing (at 1223 K (950 °C), 15 min) and austempering (543 K (270 °C), 30 min) showing a mixed mode of fracture. (b) Fractograph of the sample as obtained after impact testing.

dislocations provide ready sites for recrystallization and nucleation of ferritic shaves of bainite during austempering. This is how prior cold deformation aids creation of ultrafine or nanometric thick ferritic sheaves in bainite in the present routine. The 10 pct cold deformed samples exhibit higher impact strength than that reported by Li and Wang^[16] in samples with a similar bainite + martensite duplex microstructure obtained by isothermal treatment and subsequent water quenching of SAE 52100 steel. It should be noted that the presence of dislocation is also known to aid heterogeneous nucleation of martensite as the corresponding nucleation barrier is relatively small and the driving force is very high.^[14]

Figure 10(a) shows the scanning electron micrograph of the fractured specimen obtained after tensile deformation of a 10 pct prior cold deformed/austempered (30 minutes) sample. Localized microdimples were observed, which may be attributed to the plastic deformation of lower bainite under the influence of tensile stress. Figure 10(b) shows the fractured specimen obtained after impact testing of a sample where an identical prior cold deformation/austempering routine is followed. It is interesting to note that the failure occurs

in mixed mode in low strain rate tensile deformation, while there is a predominantly brittle fracture in the case of impact testing.

Thus, a judicious combination of prior cold deformation and austempering schedule has effectively been successful in refining the bainitic sheaves and martensite plates as well as control in the volume percent of bainite and martensite matrix. Ultrafine bainite + martensite duplex microstructure may be beneficial to deflect advancing cracks and enhance the toughness by increasing the total path length of crack propagation before ultimate fracture at a higher impact stress.

IV. CONCLUSIONS

The present study demonstrates that the optimum level of cold deformation (10 pct) prior to austenitizing (at 1223 K (950 °C) for 15 minutes) followed by austempering (at 543 K (270 °C) for 30 minutes) of SAE 52100 steel yields higher ultimate tensile (2240 MPa) and impact strength (~73 J). The tensile strength is marginally higher than the austempered steel with the same schedule without prior cold deformation.^[3] However, there has been a considerable increase in the impact strength by prior cold deformation as normal bainite + martensite duplex microstructure is reported to reach an impact strength of 53 to 60 J.^[3,16] It may be concluded that an appropriate amount of lower bainite along with martensite in SAE 52100 steel significantly enhances the toughness more than that obtained in the same steel in conventionally quenched and tempered condition (Table II). This improvement can be attributed to the typical microstructure comprising nanometric sheaves of bainitic-ferrite with embedded ultrafine carbide in them with the ferrites themselves interspaced between martensitic needles/plates.

ACKNOWLEDGMENTS

Partial financial support from Tata Steel, Jamshedpur (Project: SPI), Department of Science and Technology, New Delhi (NSTI Project No. SR/S5/NM-04/2005), and INAE Visvesvaraya Chair Professorship scheme (to I.M.) is gratefully acknowledged.

REFERENCES

1. H. Burrier: *ASM Handbook Properties and Selection of Iron Steels and High Performance Alloys*, ASM International, Materials Park, OH, 1987, vol. 1, pp. 380–88.
2. H. Bomas, T.T. Linkewitz, and P. Mayr: *Haerterei-Technische Mitteilungen*, 2002, vol. 57, pp. 190–98.
3. J. Chakraborty, D. Bhattacharjee, and I. Manna: *Scripta Mater.*, 2008, vol. 59, pp. 247–50.
4. J. Chakraborty, D. Bhattacharjee, and I. Manna: *Scripta Mater.*, 2009, vol. 61, pp. 604–07.
5. C.H. Young and H.K.D.H. Bhadeshia: *Mater. Sci. Technol.*, 1994, vol. 10, pp. 209–14.
6. J. Barford and W.S. Owen: *Met. Sci. Heat Treatment*, 1962, vol. 4, pp. 359–60.

7. M. Umemoto, K. Horiuchi, and I. Tamura: *Tetsu-to-Hagané*, 1982, vol. 68, pp. 461–70.
8. L.W. Graham and H.J. Axon: *J. Iron Steel Inst.*, 1959, vol. 191, pp. 361–65.
9. A. Matsuzaki and H.K.D.H. Bhadeshia: *Mater. Sci. Technol.*, 1999, vol. 15, pp. 518–22.
10. A.K. De, J.G. Speer, and D.K. Matlok: *Adv. Mater. Processes*, 2003, vol. 161, pp. 27–30.
11. H.K.D.H. Bhadeshia: *Bainite in Steels*, 2nd ed., Maney Publishing, London, 2001, pp. 147–54.
12. B.D. Cullity: *Elements of X-Ray Diffraction*, Addison-Wesley, Reading, MA, 1959, pp. 391–96.
13. T. Yokota, C. Garcia-Mateo, and H.K.D.H. Bhadeshia: *Scripta Mater.*, 2004, vol. 51, pp. 767–70.
14. D.A. Porter and K.E. Easterling: *Phase Transformations in Metals and Alloys*, 2nd ed., CRC Press, Broken Sound Parkway NW, Boca Raton, 2001, p. 46.
15. W.C. Oliver and G.M. Pharr: *J. Mater. Res.*, 1992, vol. 7, pp. 1564–80.
16. C. Li and J.L. Wang: *J. Mater. Sci.*, 1993, vol. 28, pp. 2112–18.
17. F. Hengerer, U. Brockmuller, and P.O. Sorstrom: *Creative Use of Bearing Steels*, ASTM Special Technical Publication-1195, ASTM, Philadelphia, PA, 1993, pp. 21–33.
18. Q. Furnémont, M. Kempf, P.J. Jacques, M. Goken, and F. Delannay: *Mater. Sci. Technol.*, 2002, vol. 328, pp. 26–32.
19. P.J. Jacques, Q. Furnémont, F. Lani, T. Pardoën, and F. Delannay: *Acta Mater.*, 2007, vol. 55, pp. 3681–93.